An *in Situ* Study of Bond Strains in 1 nm Pt Catalysts and Their Sensitivities to Cluster–Support and Cluster–Adsorbate Interactions

Anatoly I. Frenkel,*[,†] Matthew W. Small,[‡] Jeremy G. Smith,[‡] Ralph G. Nuzzo,*[,‡] Kristina O. Kvashnina,[§] and Moniek Tromp*[,‖]

[†]Physics Department, Yeshiva University, 245 Lexington Avenue, New York, New York 10016, United States

[‡]Department of Chemistry and the Frederick Seitz Materials Research Laboratory, University of Illinois in Urbana–Champaign, Urbana, Illinois 61801, United States

[§]European Synchrotron Radiation Facility (ESRF), 6 rue Jules Horowitz, BP 220, 38043 Grenoble, France

[‖]Catalyst Characterization, Catalysis Research Center, Technische Universität München, Lichtenbergstrasse 4, 85748 Garching, Germany

S *Supporting Information*

ABSTRACT: The electronic and atomic structural properties of nanoscale metal catalysts exhibit complex influences with origins related to particle size, metal–support, and metal–adsorbate interactions. The experimental investigations of these factors, as well as the elucidation of the impacts they have on mechanisms in catalysis, are hindered by their interdependency in working catalysts. We demonstrate in this work that the features underpinning bond strains and adsorbate-bonding effects in nanometer-scale Pt catalysts supported on both γ-alumina and carbon can be distinguished and analyzed using combined high-energy resolution fluorescence detection (HERFD) X-ray absorption spectroscopy methods, namely, HERFD XANES and HERFD EXAFS. The work extends insights into the fluxional structural dynamics obtained in these systems, a feature harboring significant consequences for understandings of both their properties and mechanisms of action.
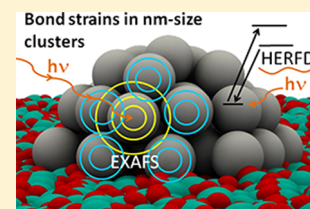
1. INTRODUCTION

Over the past few years, time-resolved and new, high-energy resolution X-ray absorption spectroscopy (XAS) methods have been used to characterize the structural and electronic properties of supported metal clusters, most notably under the *in situ* conditions in which they are used in catalysis.[1−4] These and related studies are providing insights into structure–property–rate relationships by identifying the important attributes of catalytic reaction mechanisms related to structure, linking them to specific features of particle size, atomic bonding, and electronic structure as present both *in situ* and *in operando*.[5−9] There is a growing appreciation evidenced in this literature that the structures of important classes of heterogeneous catalysts—especially those comprised of small supported metal clusters—can exhibit complex forms of fluxionality. The bonding presented by a supported cluster is also strongly impacted by the physicochemical nature of its *in operando* environment, where features of the bonding to support materials, adsorbates, and other species (promoters, poisons, etc.) can elicit bond strains sufficient to drive large-scale structural transformations. The complex interrelationships that exist within these features of the structural dynamics of supported metal cluster catalysts remain at this time incompletely understood.

The present study addresses important features of the above-noted deficiency. We consider aspects of systems for which recent synchrotron measurements[5,6] of the thermal properties of supported metal catalysts revealed a number of intriguing anomalies that do not have analogies in bulk materials. Among them are specific cases where in very small supported clusters dynamical modifications of electronic structure can produce such effects as apparent negative thermal expansion in metal–metal (M–M) bond lengths, large bond-length disorder, and strong structural perturbations related to temperature-dependent cluster–support interactions.[10] These three effects were linked to each other theoretically and highlighted the important role played by librations—fluxional nonvibrational/large amplitude atomic motions of the cluster's atoms.[10] Recent results further refined this picture by illuminating the role of adsorbates in altering the dynamic structure and electronic state of supported catalysts.[7,11] Knowledge of the dominant factors measured under the same thermodynamic conditions (i.e., at the same pressure and temperature) is required in order to understand—and perhaps tune—their catalytic properties. Many such effects can be quantitatively analyzed using *in situ* XAS. For example, the position of the d-band center relative to the Fermi level in noble metal catalysts is recognized as an important catalytic descriptor[12,13] that can also be directly related to the position and intensity of the X-ray absorption peak known as the white line.[14,15]

Several factors affect the d-band center. Bond strain, adsorbate binding, and metal–support effects are arguably the

most important of these and are the ones we examine in depth in this work. Bond strains, for example, are predicted in theory to shift the white line position,[16] and experimentally it has been shown to be a means for tailoring the catalytic activity of metals.[17] For example, compressive bond strains tend to shift the band center (and, hence, the white line) to lower energies.[13,17−19] Adsorbates (both reactants and products) that induce changes in intracluster bond relaxations and electronic structure due their bonding also can elicit shifts in the edge position.[20] In the particle size range of 1 nm, the dominant sources of strain are the interfacial stress due to the support[21] and the cluster's surface tension.[22] Because these factors dominate the observed strains, they can also mask contributions coming from more subtle sources—such as those originating in coverage-dependent adsorbate bonding interactions[7] as well as core level binding energy shifts.[23,24] Separating the effects of different sources of strain on the d-band center (and therefore the clusters' electronic structure)[16] is an important requirement, and also a formidable task, in order to fully understand the role(s) these interactions play during the course of a reaction.

The main challenge in decoupling these effects is the need to measure both electronic and structural perturbations in the same experiment under *in situ* conditions. While bond-strain magnitudes can be accessed (such as through an analysis of the bond length disorder obtained using extended X-ray absorption fine structure (EXAFS) experiments),[7,25] the electronic effects (strain- and adsorbate-induced) are only observable through correlations seen in data measured in the X-ray absorption near-edge structure (XANES) portion of the X-ray absorption spectrum. The sensitivity of all data of this form to size, shape, adsorbate, and support effects is highest for measurements made on very small particles (∼1−2 nm in size, since most atoms reside at or near a cluster boundary) and weakens as the particle size increases.

In the high energy resolution fluorescence detection (HERFD) XAS method used here, only a selected emission line is detected (as opposed to the total fluorescence yield).[26] This reduces the lifetime broadening of the spectra from the initial to final state core hole, thereby enhancing the energy resolution obtained and yielding XANES features that are better-resolved and more intense. In addition, the longer EXAFS range done in HERFD mode has been shown to enhance the structural sensitivity.[27−29] Thus, an enhanced sensitivity to changes occurring in a catalytic process can be obtained *in situ*.[26,30,31] Most importantly, acquiring both HERFD XANES and EXAFS data on small particles in the same *in situ* experiment allows direct measurements of both strain and electronic perturbations as a function of temperature and adsorbate pressure. In this work we report the results of such experiments, in which we evaluated the intracluster effects (strain) and d-band center changes in small supported Pt clusters as a function of *in situ* mediated changes in both cluster−support and cluster−adsorbate interactions. One challenge in such experiments is to correctly account for the effects of high energy resolution on EXAFS. In this work, we solved this problem by measuring the same system at two different synchrotrons, with high and low energy resolution. Synchrotron investigations were conducted *in situ* by studying Pt/γ-Al$_2$O$_3$ and Pt/C catalysts under a flow of H$_2$/He as well as CO/He mixtures at different pressures and temperatures.

2. EXPERIMENTAL DETAILS

2.1. Sample Preparation and Characterization. The Pt/γ-Al$_2$O$_3$ and the Pt/C samples were synthesized by impregnating the appropriate support material (C, Vulcan X-72, and γ-Al$_2$O$_3$ both being employed) with an aqueous solution of NH$_4$Pt(OH)$_2$ to attain a Pt loading of 0.5 wt %. After drying the samples, they were each reduced at room temperature using pure H$_2$ for 30 min prior to being heated to 773 at 3.4 K/min. This temperature was maintained for 1 h before the samples were allowed to cool back to room temperature and flushed with Ar. Particle size distributions were obtained using a JEOL 2010-F electron microscope operating in scanning transmission electron microscopy (STEM) mode.

2.2. Synchrotron X-ray Absorption Spectroscopy Measurements. X-ray absorption spectroscopy measurements were performed at the European Synchrotron Radiation Facility (ESRF) and National Synchrotron Light Source (NSLS). The ESRF experiments were performed at the high brilliance XAS/XES beamline ID26.[32] The incident energy was selected using the ⟨111⟩ reflection from a double Si crystal monochromator. Rejection of higher harmonics was achieved by three Pd/Cr mirrors at an angle of 2.5 mrad relative to the incident beam. The size of the X-ray beam was 0.3 mm (horizontal) × 1 mm (vertical). XANES spectra were simultaneously measured in total fluorescence yield mode using a photodiode and in HERFD mode using an X-ray emission spectrometer.[33] The sample, analyzer crystal, and photon detector (silicon drift diode) were arranged in a vertical Rowland geometry. The Pt HERFD spectra at the L$_3$ edge were obtained by recording the maximum intensity of the Pt L$α_1$ emission line (∼9442 eV) as a function of the incident energy. The emission energy was selected using the ⟨660⟩ reflection of four spherically bent Ge crystal analyzers (with 1 m bending radius) aligned at 80° Bragg angle. The intensity was normalized to the incident flux. A combined (incident convoluted with emitted) energy resolution of 1.8 eV was obtained as determined by measuring the full width at half-maximum (fwhm) of the elastic peak.

The NSLS experiments were performed at the beamline X18B in transmission mode, using a Si(111) double crystal monochromator. The second crystal was 20% detuned to minimize harmonics. The incident beam detector (a gas-filled ionization chamber) was filled with N$_2$, and the transmission and reference beam detectors were filled with 50% N$_2$ and 50% Ar.

2.3. *In Situ* Reactivity Studies. At the ESRF, the samples of Pt/γ-Al$_2$O$_3$ and Pt/C catalysts were loaded in a microreactor cell consisting of 0.5 mm i.d. quartz capillary, the heater block with cartridge heaters, and gas flow connections for gas input and gas analysis. Each sample was investigated at five different temperatures and three partial gas pressures. Different gas pressures were obtained by mixing H$_2$ or CO with ultrahigh purity He in different ratios: 100%, 2.5%, and 0.05% H$_2$ in He and 5%, 0.05%, and 0.005% CO in He. The total flow rates were 15 mL/min in all experiments, with the exception of the 0.005% CO in He (30 mL/min) and 2.5% H$_2$ in He (40 mL/min). Prior to the X-ray measurements, each sample was loaded into the cell and flushed under pure H$_2$ at room temperature for 30 min. The samples were then heated to 400 °C in pure H$_2$ and kept at this temperature for 20 min; subsequently, the feed was switched to the lowest (out of three) concentration of H$_2$ and kept at the same temperature until XANES data stabilized,
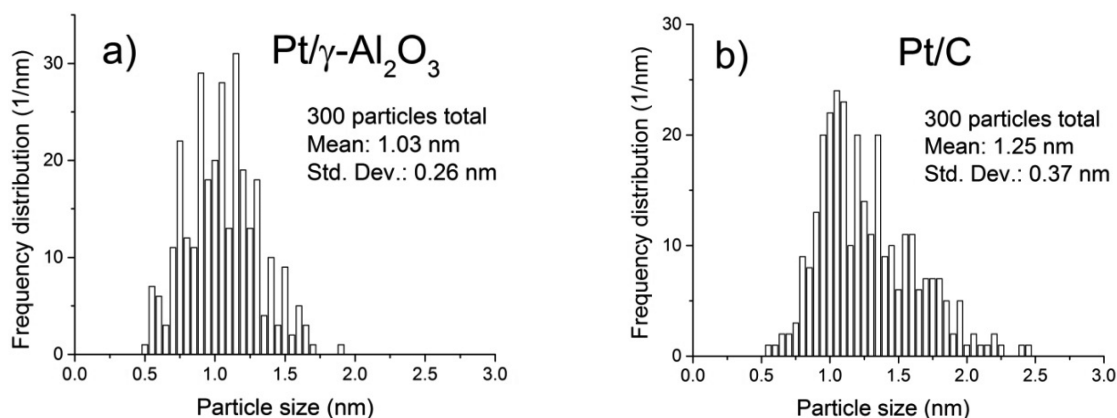
Figure 1. Particle size distributions determined by STEM: (a) Pt/γ-Al$_2$O$_3$ and (b) Pt/C.

within statistical noise. The temperature was then lowered to room temperature, and data were collected at several intermediate temperatures and room temperature. Five scans of HERFD data (from 30 eV below to 95 eV above Pt L$_3$ edge of 11564 eV) and five scans of EXAFS data (from 150 eV below to 1040 eV above Pt L$_3$ edge) were collected at each temperature. Finally, the temperature was increased back to 400 °C, and the data were remeasured at that temperature to check for system reversibility. Thus, only steady-state measurements were taken throughout the experiment. After the last scan at 400 °C, the gas concentration was increased, and the same cycle was repeated two more times. CO treatment followed H$_2$ treatment for each sample.

At the NSLS, *in situ* XAS data from the same batch of the Pt/γ-Al$_2$O$_3$ and Pt/C powders were also collected at the NSLS's X18B beamline in order to measure the coordination numbers of Pt−Pt bonds. The samples were first pressed into pellets using a 5 ton hydraulic press and mounted into a Nashner−Adler cell.[34,35] The samples were measured in transmission mode as received, then a H$_2$/He 50/50 mixture was introduced into the cell, and the samples were heated to 400 °C and held under these conditions for an hour. The samples were then cooled to room temperature and XAS measurements were taken.

## 3. STEM ANALYSIS AND VISUAL EXAMINATION OF THE HERFD DATA

3.1. Particle Size Analysis by STEM. Results of statistical analysis of particle sizes done by STEM are shown in Figure 1. The particles are similar in their average sizes (1.03 and 1.25 nm), and thus, we can focus on the effect of the substrate, temperature, and atmosphere on their properties.

3.2. HERFD XANES. The HERFD XANES data for the Pt/γ-Al$_2$O$_3$ and Pt/C samples under a variety of *in situ* conditions are shown in Figure 2a. Data taken at the high temperature (HT) limit of 673 K under either a CO or hydrogen atmosphere (500 ppm H$_2$ in He and 50 ppm CO in He) are compared in Figure 2b. The Figure 2b inset illustrates the enhanced sensitivity of HERFD XANES as compared to the total fluorescence yield detection method; the improvements evidenced there directly enable the analytical extensions described below. This enhancement is also evident from comparing the ESRF data with the NSLS data collected on the same sample and measured in transmission mode (Supporting Information Figure 1a). Figure 2a shows that significant changes in peak shape and position occur in both ambient
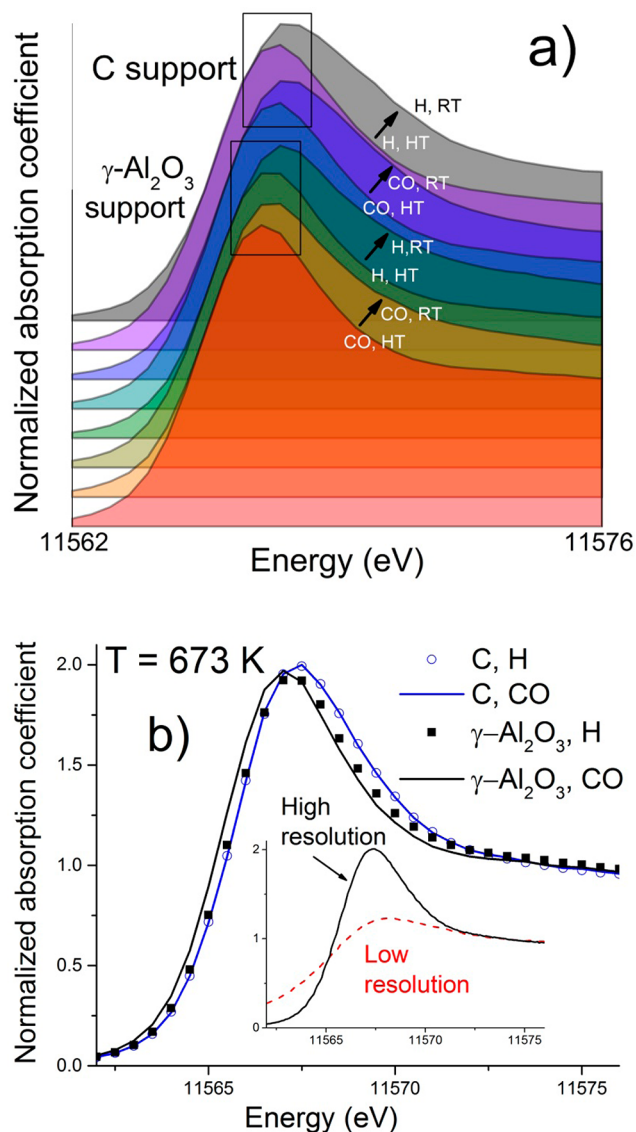
Figure 2. (a) Pt L$_3$ HERFD XANES data measured for Pt on γ-Al$_2$O$_3$ and C supports, under H$_2$ (500 ppm) or CO (50 ppm) and at RT and HT. (b) HT Pt L$_3$ HERFD XANES data from (a). Inset shows the high- and low-resolution Pt L$_3$ XANES for the Pt/C catalyst under CO at 673 K.
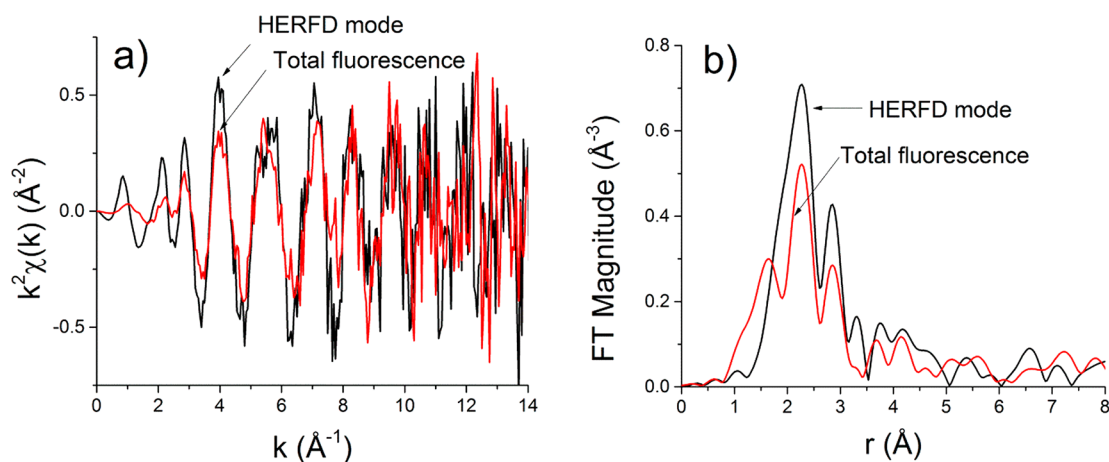
Figure 3. k^2-weighted EXAFS data for the Pt/γ-Al$_2$O$_3$ in (a) k-space and (b) r-space. The k-range of the Fourier transform window was from 3 to 11 Å^{-1}. The Hanning window function with window "sills" of 2 Å^{-1} was used in all transforms. The data were measured at ESRF in the HERFD mode and in total fluorescence mode during the flow of 0.005% CO/He at 307 K. The effect of high energy resolution over the low resolution measurement is k-dependent: the increase in intensity of oscillations is the greatest at low k values.

atmospheres as the temperature is raised from room temperature (RT) to 673 K (HT). Specifically, the peaks are shifted to the higher energy at RT compared to HT, i.e., upon addition of adsorbate, for all combinations of support and adsorbates. The strong temperature-dependent electronic changes induced in the Pt/C catalysts are particularly intriguing since previous *in situ* studies done with low-resolution XANES showed no sensitivity to H adsorbates.[35,36] These shifts are consistent with desorption of H$_2$ or CO at higher temperatures.[20,37] The adsorbate partial pressures used are high enough that a low (dynamic) coverage will be present on the Pt (one estimated to be of the order of a few percent of a monolayer at saturation based on the known heats of adsorption), and as such the high temperature data are expected to reflect a weak perturbation due to this bonding.

Figure 2b shows an overlay of the HT data for both adsorbates and supports. The data illustrate the important feature—a significant shift in the absorption edge energy—that is seen most strongly for the case of the Pt/γ-Al$_2$O$_3$ sample at HT in a low partial pressure CO environment. These data well illustrate the electronic effects on the white line position that, as we will show below, arise predominantly due to the support.

It is important to emphasize that the shift in the Pt white line position can originate from a combination of changes in different energy levels, i.e., a change in the core level energy (initial state) and/or in the unoccupied d-states that photoelectron probes by absorbing an X-ray photon. In general, this makes it difficult to pinpoint the exact reason for the shift in any particular system *a priori*. The different changes and effects are discussed in the literature extensively. One example of a core level effect is the sensitivity of the Pt white line position to the particle size and particle surface structure (both affecting the 5d band energy). In studies of Pt/γ-Al$_2$O$_3$ with metal particles in the size range of 0.8–5.4 nm,[1,2] the Pt L$_3$-edge shifted to higher energy with decreasing particle size due to the decreased coordination (and d-states depletion) of Pt atoms.[3] A positive shift of the Pt L$_3$-edge was also observed for Pt nanoparticles capped with different surfactants and demonstrates the surface effect.[3] Similarly, the metal–support interaction and metal–adsorbate interaction can both induce an edge shift.[1,4,5] For example, strongly interacting supports in which p- and/or d- orbitals of the support interact with the

particle can cause the white line position to shift. The support effect on the white line position depends on many factors, some of which are the type of support, the particle size, and particle–adsorbate interactions.

Generally speaking, both the core level and unoccupied states effects are always present in any experiment, and evaluating them separately is often difficult. Only when the white line changes are investigated systematically by varying different position-influencing, competing effects, systematically within the same experiment, one can gain insights into what factors dominate the white line behavior. Our conclusion made above, that the temperature-dependent positive shifts of the white line position are due to the changes in the Pt–adsorbate interactions, is deducible by observing two key experimental outcomes: (1) The shifts did not depend on the support. This is important to note because the interaction is weak in the case of C and strong in the case of γ-Al$_2$O$_3$. (2) The shift direction was consistent with reduced coverage for both adsorbates at higher temperatures.

We also note that, in this work, the size of the particle does not change during the experiments, since changes would have likely been irreversible, whereas all our data show excellent reversibility between different treatments. We therefore focused on discriminating between the effects of the support and the adsorbates on the white line shift measured between the lowest and the highest temperatures. These states are where the coverages are the highest and the lowest, respectively, and any adsorbate-induced effect will be in greatest contrast.

The gross trend seen in Figure 2b—that only the edge for Pt/γ-Al$_2$O$_3$ under CO shifts to lower energies compared to all other systems—is likely to be consistent with the lowering of the d-band center energy with respect to Fermi level, on the Al$_2$O$_3$ support:[38] The adsorbate coverage at 400 °C is dynamic and, due to the low partial pressure of adsorbates, is negligible (*vide supra*). The white line energy difference can thus occur due to either the charge transfer from the support onto the metal or the change in the d-band due to the strain, or both. We note that, regardless of the specific form of particle–support interaction responsible for this shift, the distinction between the Pt/γ-Al$_2$O$_3$ and Pt/C samples cannot arise as a consequence of a size difference given that the average particle sizes for both systems are similar. Distinctions in electronic

structure—as demonstrated here—can also be reflected in attributes of atomic structure (specifically bond length compression and strain). We quantitatively evaluated this possibility using data from our HERFD EXAFS measurements.

3.3. HERFD EXAFS. Advantages of HERFD's high energy resolution are clearly seen in the EXAFS data (Figure 3 and Supporting Information Figure 1b,c), especially in the lowest k region that immediately follows the XANES portion of energy range.

As in the XANES, the EXAFS spectra have higher intensity of oscillations in the HERFD mode, and the r-space peaks are also more intense, as expected. Graphs of all EXAFS data collected at the ESRF in HERFD mode at different temperatures are shown in Supporting Information Figure 2. Representative r-space EXAFS spectra of Pt/γ-Al$_2$O$_3$ and Pt/C samples show large differences in the Pt−Pt peak intensities between the two supports (Figure 4). The data are shown at
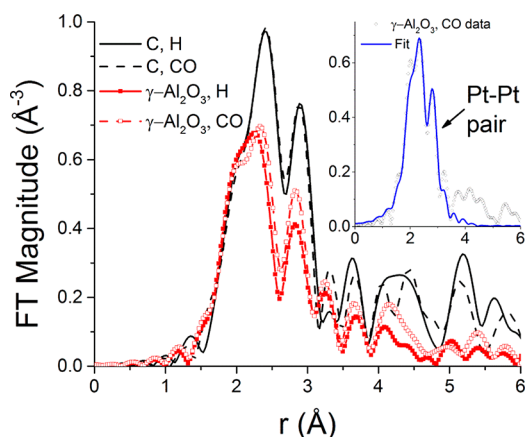
Figure 4. HERFD EXAFS data at RT, shown in r-space, for Pt clusters on C and γ-Al$_2$O$_3$ supports under H$_2$ (500 ppm) or CO (50 ppm). The k-range from 2 to 12 Å^{-1} and k^2 weighting were used for all Fourier transforms. Fit quality for the data is demonstrated in the inset for the alumina-supported Pt clusters in 50 ppm CO at RT. The k-range in the Fourier transform of the data and the fit was from 3 to 12.5 Å^{-1}.

room temperature, and hence, the difference in thermal Pt−Pt bond length disorder cannot explain this observation. On the other hand, the static (configuration) disorder can be—and almost certainly will be—different between the two catalysts.[7,36] Another possible explanation of this differing intensity is the change in coordination number (CN) caused by comparing different sized/shaped clusters.[35,39,40] In order to distinguish between the effects of disorder and the coordination number on EXAFS intensity, quantitative analysis is needed.

4. EXAFS DATA ANALYSIS AND RESULTS

The first step in structural refinement of HERFD data is to correct for the high energy resolution effect that causes enhancement of the oscillation intensity at low k (Figure 3) and is not taken into account in the EXAFS equation for the first-nearest-neighbor (1NN) coordination shell:[41]

$$\chi(k) = \frac{S_0^2 N}{kR^2} |f^{\text{eff}}(k)| \sin[2kR + \delta(k)] e^{-2\sigma^2 k^2} e^{-2R/\lambda(k)}$$

(1)

In eq 1, the passive electron reduction factor, S_0^2, the Pt−Pt coordination number, N, and the Pt−Pt bond length disorder,

σ^2, all contribute to the oscillation amplitude. Hence, they will not be reliably determined unless the energy resolution effect (which correlates with these other amplitude factors) is accounted for in the data analysis. This can be done by introducing an imaginary energy shift ΔE_i that corrects for experimental broadening effects.[42] In order to minimize the correlation of amplitude factors in eq 1, we measured data in the same samples using transmission mode at the NSLS X18B beamline. Supporting Information Figure 1 demonstrates good agreement between the total fluorescence yield data measured at the ESRF and the transmission data measured at the NSLS. Both data sets are notably lower in intensity than the ESRF data measured in HERFD mode, as expected. The NSLS transmission data was of superior quality compared to the total fluorescence data measured at the ESRF, thus validating our approach. The S_0^2 factor was found to be 0.85 by fitting the Pt foil EXAFS data and then fixed for the nanocatalyst data analysis. As a result, we obtained the Pt−Pt CNs from the fits to the NSLS EXAFS data for both the Pt/γ-Al$_2$O$_3$ and Pt/C samples (8.2 and 8.6, respectively, *vide infra*) and then fixed these values in the analysis of the high resolution EXAFS data measured at the ESRF. This is a conservative approach compared to a more general model of analysis where both the CNs and the bond length disorder parameters were allowed to vary. The former can change due to, e.g., shape change[7] or coarsening[43] of the particles and the latter due to the dynamic disorder that increases with temperature.[44] Since the changes in the data were obtained to be reversible upon thermal cycling at all regimes studied in this work, the particle coarsening should be ruled out. Furthermore, the shape change, if present, would not have affected the coordination numbers more than 15% for the particle sizes in the range in 1−1.5 nm range.[7] The 15% is within the uncertainty of the coordination number measurements by our method (Table 1). Hence, we fixed the coordination numbers to be constant in the analysis of temperature-dependent data.

Table 1. Pt−Pt Bond Characteristics (Coordination Numbers, Mean Distances, and Their Second and Third Cumulants) for the Pt Foil and the Two NP Samples Measured at the NSLS Beamline X18B at Room Temperature after the 50/50 H$_2$/He Reduction at 400 °C

sample	N(Pt−Pt)	R (Å)	σ^2 (Å^2)	$\sigma^{(3)}$ (Å^3)
Pt/γ-Al$_2$O$_3$	8.2(1.3)	2.75(2)	0.0092(11)	0.00035(27)
Pt/C	8.6(1.0)	2.748(6)	0.0073(7)	N/A
Pt foil	12	2.767(4)	0.0049(1)	0.00002(3)

In principle, the total fluorescence data measured in the HERFD experiment would have been a good alternative to our approach for EXAFS analysis since both signals (the total fluorescence and HERFD spectra) are measured simultaneously. However, in the ESRF experiment, we used a small area detector for total fluorescence, and the corresponding data (Figure 3) were not of sufficiently high quality for quantitative EXAFS analysis. For example, the background subtraction problem due to the noise in the data results in the low r peak observed at ~1.5 Å in the total fluorescence EXAFS data shown in Figure 3b.

The correlation between ΔE_i and σ^2 was minimized by using a multiple data set analysis where ΔE_i was constrained to be the same at all temperatures (because the energy resolution effects are caused by the instrument and thus are temperature-
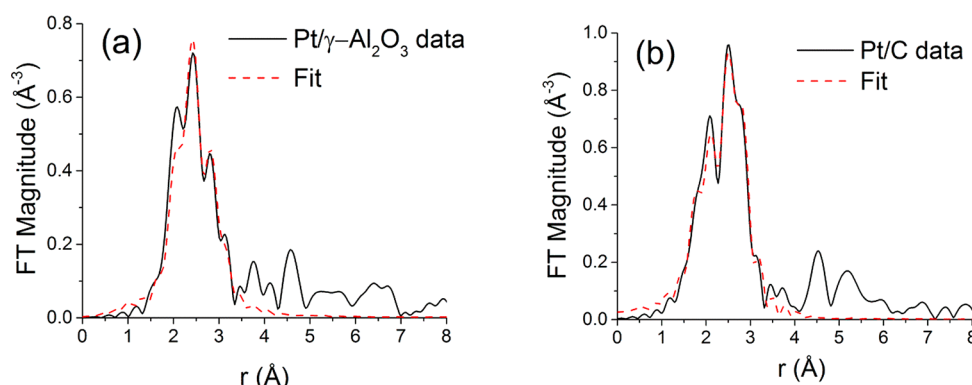
Figure 5. Fourier transform magnitudes of the k^2-weighted EXAFS spectra collected at the NSLS at room temperature and theoretical fits for the Pt/γ-Al$_2$O$_3$ (a) and Pt/C (b).

independent). In this method, several data sets are refined concurrently, where the fitting model uses the same global variables for all data sets as well as some variables specific to each set. The global variables kept the same for all temperatures were the energy origin correction ΔE_0 and imaginary energy shift ΔE_i. The Pt−Pt distance corrections, the bond length disorders, and the third cumulants were varied independently for each temperature. The typical k-ranges were from 2.5 to 12 Å^{-1} at room temperature data and 2.5 to 9.5 Å^{-1} at the 673 K data, and the typical r-range was between 1.6 and 3.2 Å. With this approach, the total number of data points was 43 in a typical fit, and the total number of variables was 17, i.e., much smaller than the number of data points. The best fit results for the ΔE_i (ca. −2.0 eV for all data analyzed in this work) validate the use of this parameter in the fit since it accounts for "negative broadening" of the experimental data with respect to FEFF theory. Representative data and fits are shown in Figure 4 (inset). All data and fits in r-space for both magnitude and real part of Fourier transforms are shown in Supporting Information Figures 2−6. Best fit values of all parameters varied in the fits are reported in Supporting Information Table 1.

For the analysis of the data collected at the NSLS, the fits for Pt/C sample were performed using the k-range from 2.9 to 14.1 Å^{-1}. The r-range was from 1.4 to 3.4 Å. The fitting variables included the correction to the photoelectron energy origin, the Pt−Pt coordination number, the distance correction, and the disorder in the distance. In addition, the Pt−C pair was included in the fit, and the coordination number, distance correction, and the disorder were also varied in the fit. The total number of relevant independent data points was 14, and the total number of variables was 7. The fits for the Pt/γ-Al$_2$O$_3$ sample were performed using the k-range from 2.6 to 13.7 Å^{-1}. The r-range was from 1.6 to 3.3 Å. The total number of relevant independent data points was 12, and the total number of variables was 5. Fourier transform magnitudes of the representative data and fits are shown in Figure 5. Supporting Information Figure 7 shows real parts of Fourier transforms of the data and fits for the both samples measured at the NSLS. Numerical results for the Pt−Pt bond lengths and their disorder are reported in Table 1. For the Pt/C sample, the Pt−C coordination number was found to be 1.4 ± 0.8, the bond length 2.15 ± 0.02 Å, and its disorder 0.004 ± 0.005 Å^2. Because of the large uncertainties in the coordination number and disorder parameter, the Pt−C contribution does not affect the fit significantly and is not discussed.

5. RESULTS OF EXAFS ANALYSIS

Quantitative results for 1NN Pt−Pt distances are shown in Figure 6. Pt/C catalysts show relatively large Pt−Pt distances
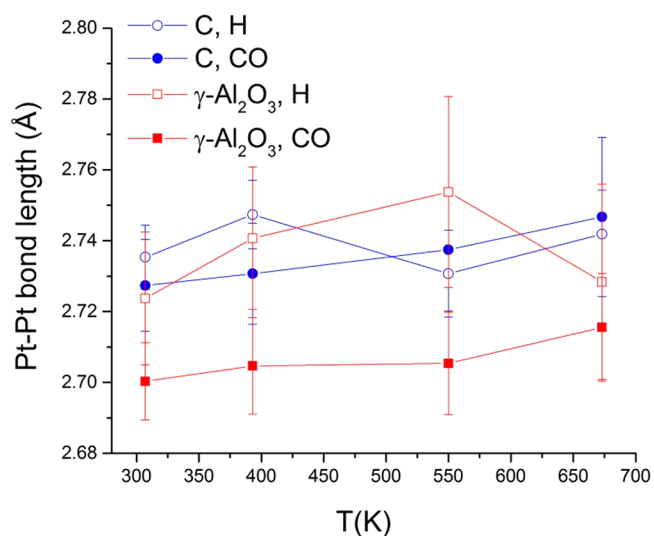
Figure 6. 1NN Pt−Pt distances obtained by EXAFS analysis.

that, consistent with the XANES behavior in the same samples (Figure 2b), have very weak sensitivity to adsorbates. In striking contrast to the carbon-supported samples, alumina-supported particles show strong 1NN Pt−Pt distance dependencies on the adsorbate gas. It is also evident that the CO environment causes this distance to decrease significantly compared to a hydrogen environment.

This contrast is also in excellent agreement with the XANES behavior of the same Pt/γ-Al$_2$O$_3$ sample, where the white line positions were found to be very different for H and CO adsorbates, while for the Pt/C sample they were identical (Figure 2b).

Figure 7 shows the 1NN Pt−Pt bond length disorder as a function of temperature for both samples and adsorbates. The data obtained in bulk Pt foil[6] are shown for reference purposes.

6. DISCUSSION

Disorder in nanoclusters can be described using an approximation that the static (σ_s^2) and dynamic (σ_d^2) bond length disorders are statistically independent. This allows the static disorder to be separated from the total disorder using the
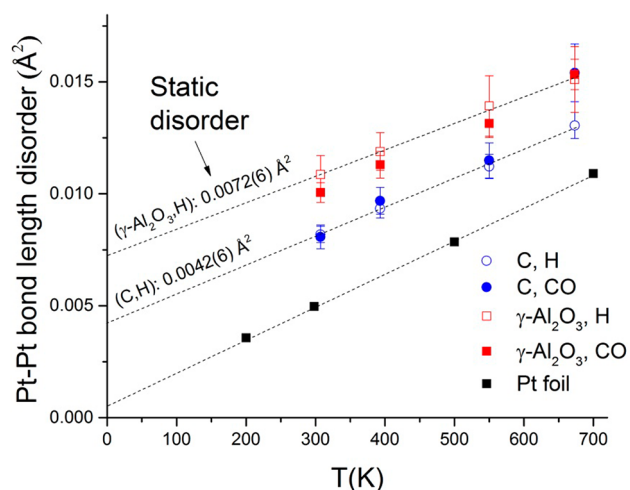
Figure 7. 1NN Pt−Pt bond length disorder (symbols) and linear fit with eq 2 (lines) for supported Pt nanoparticle samples and bulk Pt foil (ref 6).

system's temperature dependence in the HT (above Einstein temperature) limit:[35]

$$\sigma^2 \approx \sigma_s^2 + k_B T/k \qquad (2)$$

where k_B is the Boltzmann's constant and k is the effective Pt−Pt force constant. Table 2 contains the best fit values for the Pt−Pt force constants and the static disorder. The small positive y-intercept of 0.0006 Å^2 for Pt foil (Figure 7) indicates the level of experimental uncertainty for σ_s^2. Using the experimentally measured values for N, k, and σ_s^2, we can evaluate the residual (static) elastic strain energy per Pt atom:[7,25]

$$W = \frac{1}{2} N k \sigma_s^2 \qquad (3)$$

Cluster strain energies calculated for both supports and atmospheres are tabulated in Table 2. They are in good agreement with previously obtained strain energies for clusters supported on γ-Al$_2$O$_3$.[7]

The most important feature of this latter sensitivity is that the magnitude of this strain energy is always larger for the Al$_2$O$_3$ support compared to the C support at similar conditions. We note that the strain calculations were done over the range of temperatures during which the coverage of CO and H on the Pt clusters varies from saturation to a few percent of a monolayer.[7] Therefore, this result strongly supports the hypothesis that both a bond-mediated compressive strain (not originating from metal−adsorbate bonding) and the significant shift of the Pt L$_3$ white line seen in the XANES data of Figure 2b for Pt clusters on the alumina support at HT under CO share the same origin.

The fact that the strain is compressive, not tensile, is obvious from Figure 6, which shows that the average Pt−Pt bonds,

under a CO atmosphere, are shorter for the γ-Al$_2$O$_3$ support. In contrast, both supports show no shortening (outside the uncertainties) of the Pt−Pt bonds for the samples under a hydrogen environment.

For most metals, it is now well appreciated that very small particle sizes, such as in the 1 nm diameter range considered here, lead to generally compressive strains in the M−M bonding. These contractions are dominated by bond relaxations occurring at surface/low coordination number sites.[22] Adsorbates also play a key role in mediating surface M−M bond relaxations, for example in lengthening M−M bonds at high coverages of H.[45] We see in the present work, however, that a very persistent strain is evidenced in the high temperature limit where (at partial pressures of H$_2$ and CO used) the adsorbate coverages are very low. The current data establish that the large strains seen for Pt/γ-Al$_2$O$_3$ arise predominantly from the specific chemistry of the particle−support interactions.

The chemistry underlying this effect is related to the physical state of the alumina support being altered from that present under ambient conditions. It is well-known that Pt clusters promote the formation of strongly bound hydrogen sites on the alumina support. At low partial pressures of H$_2$ coverage of these strongly bound forms—frequently described as support hydroxylation—will remain high. In CO, however, heating in an environment devoid of H sources (e.g., H$_2$, H$_2$O, etc.) leads to an irreversible desorption process of H$_2$ from the surfaces present that must eventually deplete these sites. (No such effects are seen for Pt/C, naturally, given the absence of similar support-mediated bonding.) Hence, both the compressive strain and the significant edge shift seen at HT for Pt/γ-Al$_2$O$_3$ under CO compared to H$_2$ arises, we believe, due to different surface states of the support being present in H$_2$ and CO environments at HT. We believe that this difference fully explains the character of the bond strains and perturbations of the energetics seen in the Pt/γ-Al$_2$O$_3$ data. Notably, the addition of H to support-mediated bonding environments must serve to increase electron density on Pt, as seen in the XANES data, and as seen in the EXAFS data, these interactions do in fact lift the bond compression in the clusters by increasing net charge exchange to the metal. Since the perturbations of the d-band occupancy this engenders must arise very locally, the affected sites must be ones proximate to or in direct contact with the Pt clusters. We should note that there exists a considerable literature suggesting that O atom vacancies very likely play a strong role in this bonding. The present data provide little guidance as to the atomistics involved or how to couple this aspect of bonding to the binding motifs of H implicated here. Theory and atomic resolution environmental electron microscopy studies provide two means to better resolve these outstanding questions.

7. SUMMARY

Our measurements show that the bond strain is predominantly affected by the particle−support interaction. Still, we cannot

Table 2. Pt−Pt Force Constant, Static Disorder, and Cluster Strain Energy (per Pt Atom), Obtained for Different Supports and Adsorbates

support	H$_2$			CO		
	k (N/m)	σ_s^2 (Å^2)	W (kJ/mol)	k (N/m)	σ_s^2 (Å^2)	W (kJ/mol)
C	105(4)	0.0042(6)	11(2)	80(2)	0.003(1)	6(2)
γ-Al$_2$O$_3$	116(4)	0.0072(6)	22(2)	100(5)	0.0058(6)	15(2)

quantitatively separate the contributions of the support and the particle's surface tension to the total strain measured in this work (Table 2), since the particle sizes in both cases were similar. This work highlights the need for theoretical modeling that will take into account all components of this complex system. These results also demonstrate the significant sharpening and increased intensity obtainable with *in situ* HERFD (both XANES and EXAFS) data, which can be critical for detecting the substrate and ligand effects in future studies of catalysts.

■ ASSOCIATED CONTENT

Ⓢ Supporting Information

Comparison between the EXAFS data measured in transmission and fluorescence (with high energy resolution); EXAFS data in *k*-space; EXAFS data and fits in *r*-space; results for the Pt−Pt bond lengths and mean-square bond length disorder factors. This material is available free of charge via the Internet at http://pubs.acs.org.

■ AUTHOR INFORMATION

Corresponding Authors
*E-mail anatoly.frenkel@yu.edu (A.I.F.).
*E-mail r-nuzzo@illinois.edu (R.G.N.).
*E-mail moniek.tromp@tum.de (M.T.).

Notes
The authors declare no competing financial interest.

■ ACKNOWLEDGMENTS

■ REFERENCES

(1) Dent, A. J.; Evans, J.; Fiddy, S. G.; Jyoti, B.; Newton, M. A.; Tromp, M. Rhodium Dispersion during NO/CO Conversions. *Angew. Chem., Int. Ed.* **2007**, *46*, 5356−5358.

(2) Singh, J.; Alayon, E. M. C.; Tromp, M.; Safonova, O. V.; Glatzel, P.; Nachtegaal, M.; Frahm, R.; van Bokhoven, J. A. Generating Highly Active Partially Oxidized Platinum during Oxidation of Carbon Monoxide over Pt/Al₂O₃: In Situ, Time-Resolved, and High-Energy-Resolution X-Ray Absorption Spectroscopy. *Angew. Chem., Int. Ed.* **2008**, *47*, 9260−9264.

(3) Grunwaldt, J.-D.; Kimmerle, B.; Baiker, A.; Boye, P.; Schroer, C. G.; Glatzel, P.; Borca, C. N.; Beckmann, F. Catalysts at Work: From Integral to Spatially Resolved X-Ray Absorption Spectroscopy. *Catal. Today* **2009**, *145*, 267−278.

(4) Merte, L. R.; Behafarid, F.; Miller, D. J.; Friebel, D.; Cho, S.; Mbuga, F.; Sokaras, D.; Alonso-Mori, R.; Weng, T.-C.; Nordlund, D.; et al. Electrochemical Oxidation of Size-Selected Pt Nanoparticles Studied Using in Situ High-Energy-Resolution X-Ray Absorption Spectroscopy. *ACS Catal.* **2012**, *2*, 2371−2376.

(5) Kang, J. H.; Menard, L. D.; Nuzzo, R. G.; Frenkel, A. I. Unusual Non-bulk Properties in Nanoscale Materials: Thermal Metal-Metal Bond Contraction of gamma-Alumina-Supported Pt Catalysts. *J. Am. Chem. Soc.* **2006**, *128*, 12068−12069.

(6) Sanchez, S. I.; Menard, L. D.; Bram, A.; Kang, J. H.; Small, M. W.; Nuzzo, R. G.; Frenkel, A. I. The Emergence of Nonbulk Properties in Supported Metal Clusters: Negative Thermal Expansion and Atomic Disorder in Pt Nanoclusters Supported on gamma-Al₂O₃. *J. Am. Chem. Soc.* **2009**, *131*, 7040−7054.

(7) Small, M. W.; Sanchez, S. I.; Marinkovic, N. S.; Frenkel, A. I.; Nuzzo, R. G. Influence of Adsorbates on the Electronic Structure, Bond Strain, and Thermal Properties of an Alumina-Supported Pt Catalyst. *ACS Nano* **2012**, *6*, 5583−5595.

(8) Cuenya, B. R.; Frenkel, A. I.; Mostafa, S.; Behafarid, F.; Croy, J. R.; Ono, L. K.; Wang, Q. Anomalous Lattice Dynamics and Thermal Properties of Supported Size- and Shape-Selected Pt Nanoparticles. *Phys. Rev. B* **2010**, *82*, 155450.

(9) Paredis, K.; Ono, L. K.; Mostafa, S.; Li, L.; Zhang, Z. F.; Yang, J. C.; Barrio, L.; Frenkel, A. I.; Cuenya, B. R. Structure, Chemical Composition, and Reactivity Correlations during the in Situ Oxidation of 2-Propanol. *J. Am. Chem. Soc.* **2011**, *133*, 6728−6735.

(10) Vila, F.; Rehr, J. J.; Kas, J.; Nuzzo, R. G.; Frenkel, A. I. Dynamic Structure in Supported Pt Nanoclusters: Real-Time Density Functional Theory and X-Ray Spectroscopy Simulations. *Phys. Rev. B* **2008**, *78*, 121404 R.

(11) Behafarid, F.; Ono, L. K.; Mostafa, S.; Croy, J. R.; Shafai, G.; Hong, S.; Rahman, T. S.; Bare, S. R.; Cuenya, B. R. Electronic Properties and Charge Transfer Phenomena in Pt Nanoparticles on gamma-Al₂O₃: Size, Shape, Support, and Adsorbate Effects. *Phys. Chem. Chem. Phys.* **2012**, *14*, 11766−11779.

(12) Hammer, B.; Norskov, J. K. Electronic Factors Determining the Reactivity of Metal Surfaces. *Surf. Sci.* **1995**, *343*, 211−220.

(13) Hammer, B.; Norskov, J. K. Theoretical Surface Science and Catalysis - Calculations and Concepts. *Adv. Catal.* **2000**, *45*, 71−129.

(14) Mansour, A. N.; Cook, J. W.; Sayers, D. E. Quantitative Technique for the Determination of the Number of Unoccupied d-Electron States in a Platinum Catalyst Using the L₂,₃ X-Ray Absorption Edge Spectra. *J. Phys. Chem.* **1984**, *88*, 2330−2334.

(15) Yoo, S. J.; Hwang, S. J.; Lee, J.-G.; Lee, S.-C.; Lim, T.-H.; Sung, Y.-E.; Wieckowski, A.; Kim, S.-K. Promoting Effects of La for Improved Oxygen Reduction Activity and High Stability of Pt on Pt-La Alloy Electrodes. *Energy Environ. Sci.* **2012**, *5*, 7521−7525.

(16) Shao, M. H.; Huang, T.; Liu, P.; Zhang, J.; Sasaki, K.; Vukmirovic, M. B.; Adzic, R. R. Palladium Monolayer and Palladium Alloy Electrocatalysts for Oxygen Reduction. *Langmuir* **2006**, *22*, 10409−10415.

(17) Mavrikakis, M.; Hammer, B.; Nørskov, J. K. Effect of Strain on the Reactivity of Metal Surfaces. *Phys. Rev. Lett.* **1998**, *81*, 2819−2822.

(18) Greeley, J.; Norskov, J. K.; Mavrikakis, M. Electronic Structure and Catalysis on Metal Surfaces. *Annu. Rev. Phys. Chem.* **2002**, *53*, 319−348.

(19) Kitchin, J. R.; Nørskov, J. K.; Barteau, M. A.; Chen, J. G. Role of Strain and Ligand Effects in the Modification of the Electronic and Chemical Properties of Bimetallic Surfaces. *Phys. Rev. Lett.* **2004**, *93*, 156801.

(20) Guo, N.; Fingland, B. R.; Williams, W. D.; Kispersky, V. F.; Jelic, J.; Delgass, W. N.; Ribeiro, F. H.; Meyer, R. J.; Miller, J. T. Determination of CO, H₂O and H₂ Coverage by XANES and EXAFS on Pt and Au during Water Gas Shift Reaction. *Phys. Chem. Chem. Phys.* **2010**, *12*, 5678−5693.

(21) Schebarchov, D.; Hendy, S. C. Effects of Epitaxial Strain on the Melting of Supported Nickel Nanoparticles. *Phys. Rev. B* **2011**, *84*, 085407.

(22) Vermaak, J. S.; Mays, C. W.; Kuhlmann-Wilsdorf, D. On Surface Stress and Surface Tension: I. Theoretical Considerations. *Surf. Sci.* **1968**, *12*, 128−133.

(23) Nozieres, P.; De Dominicis, C. T. Singularities in X-Ray Absorption and Emission of Metals. 3. One-Body Theory Exact Solution. *Phys. Rev.* **1969**, *178*, 1097−1107.

(24) Johansson, B.; Martensson, N. Core-Level Binding-Energy Shifts for the Metallic Elements. *Phys. Rev. B* **1980**, *21*, 4427−4457.

(25) Frenkel, A. I.; Stern, E. A.; Voronel, A.; Heald, S. M. Lattice Strains in Disordered Mixed Salts. *Solid State Commun.* **1996**, *99*, 67−71.

(26) Safonova, O. V.; Tromp, M.; van Bokhoven, J. A.; de Groot, F. M. F.; Evans, J.; Glatzel, P. Identification of CO Adsorption Sites in Supported Pt Catalysts Using High-Energy-Resolution Fluorescence Detection X-ray Spectroscopy. *J. Phys. Chem. B* **2006**, *110*, 16162–16164.

(27) Yano, J.; Pushkar, Y.; Glatzel, P.; Lewis, A.; Sauer, K.; Messinger, J.; Bergmann, U.; Yachandra, V. High-Resolution Mn EXAFS of the Oxygen-Evolving Complex in Photosystem II: Structural Implications for the Mn_4Ca Cluster. *J. Am. Chem. Soc.* **2005**, *127*, 14974–14975.

(28) Pushkar, Y.; Yano, J.; Glatzel, P.; Messinger, J.; Lewis, A.; Sauer, K.; Bergmann, U.; Yachandra, V. Structure and Orientation of the Mn_4Ca Cluster in Plant Photosystem II Membranes Studied by Polarized Range-Extended X-Ray Absorption Spectroscopy. *J. Biol. Chem.* **2007**, *282*, 7198–7208.

(29) Yano, J.; Kern, J.; Pushkar, Y.; Sauer, K.; Glatzel, P.; Bergmann, U.; Messinger, J.; Zouni, A.; Yachandra, V. K. High-Resolution Structure of the Photosynthetic Mn_4Ca Catalyst from X-Ray sSpectroscopy. *Philos. Trans. R. Soc., B* **2008**, *363*, 1139–1147.

(30) Bordiga, S.; Groppo, E.; Agostini, G.; van Bokhoven, J. A.; Lamberti, C. Reactivity of Surface Species in Heterogeneous Catalysts Probed by in Situ X-Ray Absorption Techniques. *Chem. Rev.* **2013**, *113*, 1736–1850.

(31) Glatzel, P.; Singh, J.; Kvashnina, K. O.; van Bokhoven, J. A. In Situ Characterization of the 5d Density of States of Pt Nanoparticles upon Adsorption of CO. *J. Am. Chem. Soc.* **2010**, *132*, 2555–2557.

(32) Signorato, R.; Sole, V. A.; Gauthier, C. Performance of the ESRF ID26 Beamline Reflective Optics. *J. Synchrotron Radiat.* **1999**, *6*, 176–178.

(33) Glatzel, P.; Bergmann, U. High Resolution 1s Core Hole X-Ray Spectroscopy in 3d Transition Metal Complexes—Electronic and Structural Information. *Coord. Chem. Rev.* **2005**, *249*, 65–95.

(34) Nashner, M. S.; Frenkel, A. I.; Adler, D. L.; Shapley, J. R.; Nuzzo, R. G. Structural Characterization of Carbon-Supported Platinum-Ruthenium Nanoparticles from the Molecular Cluster Precursor $PtRu_5C(CO)_{16}$. *J. Am. Chem. Soc.* **1997**, *119*, 7760–7771.

(35) Frenkel, A. I.; Hills, C. W.; Nuzzo, R. G. A View from the Inside: Complexity in the Atomic Scale Ordering of Supported Metal Nanoparticles. *J. Phys. Chem. B* **2001**, *105*, 12689–12703.

(36) Small, M. W.; Sanchez, S. I.; Menard, L. D.; Kang, J. H.; Frenkel, A. I.; Nuzzo, R. G. The Atomic Structural Dynamics of gamma-Al_2O_3 Supported Ir-Pt Nanocluster Catalysts Prepared from a Bimetallic Molecular Precursor: A Study Using Aberration-Corrected Electron Microscopy and X-Ray Absorption Spectroscopy. *J. Am. Chem. Soc.* **2011**, *133*, 3582–3591.

(37) Bolin, T. B.; Wu, T.; Schweitzer, N.; Lobo-Lapidus, R.; Kropf, A. J.; Wang, H.; Hu, Y.; Miller, J. T.; Heald, S. M. In Situ Intermediate-Energy X-Ray Catalysis Research at the Advanced Photon Source Beamline 9-BM. *Catal. Today* **2013**, *205*, 141–147.

(38) Serp, P.; Philippot, K. *Nanomaterials in Catalysis*; Wiley-VCH: Weiheim, 2013.

(39) Frenkel, A. Solving the 3D Structure of Metal Nanoparticles. *Z. Kristallogr.* **2007**, *222*, 605–611.

(40) Cuenya, B. R.; Croy, J. R.; Mostafa, S.; Behafarid, F.; Li, L.; Zhang, Z. F.; Yang, J. C.; Wang, Q.; Frenkel, A. I. Solving the Structure of Size-Selected Pt Nanocatalysts Synthesized by Inverse Micelle Encapsulation. *J. Am. Chem. Soc.* **2010**, *132*, 8747–8756.

(41) Zabinsky, S. I.; Rehr, J. J.; Ankudinov, A.; Albers, R. C.; Eller, M. J. Multiple-Scattering Calculations of X-Ray-Absorption Spectra. *Phys. Rev. B* **1995**, *52*, 2995–3009.

(42) Kelly, S. D.; Bare, S. R.; Greenlay, N.; Azevedo, G.; Balasubramanian, M.; Barton, D.; Chattopadhyay, S.; Fakra, S.; Johannessen, B.; Newville, M.; et al. Comparison of EXAFS Foil Spectra from Around the World. *J. Phys.: Conf. Ser.* **2009**, *190*, 012032.

(43) Matos, J.; Ono, L. K.; Behafarid, F.; Croy, J. R.; Mostafa, S.; DeLaRiva, A. T.; Datye, A. K.; Frenkel, A. I.; Roldan Cuenya, B. In Situ Coarsening Study of Inverse Micelle-Prepared Pt Nanoparticles Supported on gamma-Al_2O_3: Pretreatment and Environmental Effects. *Phys. Chem. Chem. Phys.* **2012**, *14*, 11457–11467.

(44) Frenkel, A. I.; Rehr, J. J. Thermal Expansion and X-Ray-Absorption Fine-Structure Cumulants. *Phys. Rev. B* **1993**, *48*, 585–588.

(45) Wang, L.-L.; Johnson, D. D. Shear Instabilities in Metallic Nanoparticles: Hydrogen-Stabilized Structure of Pt_{37} on Carbon. *J. Am. Chem. Soc.* **2007**, *129*, 3658–3664.